Exciton confinement in strain-engineered metamorphic InAs/In$_x$Ga$_{1-x}$As quantum dots

S. A. Khattak,[1,2] M. Hayne,[1] J. Huang,[3] J. Vanacken,[3] V. V. Moshchalkov,[3] L. Seravalli,[4] G. Trevisi,[4] and P. Frigeri[4]

[1]*Department of Physics, Lancaster University, Lancaster LA1 4YB, United Kingdom*
[2]*Department of Physics, Abdul Wali Khan University Mardan, Mardan 23200, Pakistan*
[3]*Institute for Nanoscale Physics and Chemistry (INPAC), Katholieke Universiteit Leuven, Celestijnenlaan 200D, B-3001 Leuven, Belgium*
[4]*IMEM-CNR, Institute of Materials for Electronics and Magnetism, Parco Area delle Scienze 37/A, I-43124 Parma, Italy*

We report a comprehensive study of exciton confinement in self-assembled InAs quantum dots (QDs) in strain-engineered metamorphic In$_x$Ga$_{1-x}$As confining layers on GaAs using low-temperature magnetophotoluminescence. As the lattice mismatch (strain) between QDs and confining layers (CLs) increases from 4.8% to 5.7% the reduced mass of the exciton increases, but saturates at higher mismatches. At low QD-CL mismatch there is clear evidence of spillover of the exciton wave function due to small localization energies. This is suppressed as the In content x in the CLs decreases (mismatch and localization energy increasing). The combined effects of low effective mass and wave-function spillover at high x result in a diamagnetic shift coefficient that is an order of magnitude larger than for samples where In content in the barrier is low (mismatch is high and localization energy is large). Finally, an anomalously small measured Bohr radius in samples with the highest x is attributed to a combination of thermalization due to low localization energy, and its enhancement with magnetic field, a mechanism which results in small dots in the ensemble dominating the measured Bohr radius.

I. INTRODUCTION

Self-assembled quantum dots (QDs) have been the subject of intense investigation for decades, and can be exploited in a variety of technologies [1–3]. Due to the confinement of carriers in all three spatial directions, they promise improved performance in applications such as infrared photodetectors [4], low-threshold lasers [5], optical amplifiers [6], memory devices [7], and single-photon sources [8]. Self-assembled QDs are spontaneously formed when a few monolayers (MLs) of crystalline material are grown epitaxially on a substrate with lattice mismatch of a few percent (Stranski-Krastanow growth) [9]. These nanostructures have many advantages, including large confinement energies and energy-level separations, high radiative efficiency, high areal densities, and good uniformity, while their inclusion in a semiconductor matrix readily permits the efficient injection and extraction of carriers [10].

An important technological goal of research on QDs has been the development of lasers with emission at telecommunications wavelengths, i.e., 1.3–1.6 μm [11–13]. Many approaches have been adopted to extend the wavelength beyond the ~1100 nm that is naturally reached by InAs QDs in GaAs. These typically involve introducing materials that increase the QD size or reduce the strain, which, in turn, lowers the energies of the confined states in the QD [14–17]. For example, decreasing the growth rate of InAs [18,19] and the use of atomic layer molecular beam epitaxy (ALMBE) [20] are both effective methods to increase QD size [21,22].

Another route to extend the emission wavelength is the use of strain-engineered metamorphic In$_x$Ga$_{1-x}$As confining layers (CLs) on GaAs, into which the InAs QDs are embedded [23–25]. Several groups have produced ~1.5-μm-wavelength lasers by this method [26,27], and in a recent work, telecoms-wavelength single-photon emission was demonstrated, with encouraging results for the generation of entangled pairs of photons [28]. In$_x$Ga$_{1-x}$As CLs have reduced lattice mismatch with the InAs QDs compared to GaAs, and also a lower

band discontinuity with InAs, redshifting the QD emission. QD sizes are affected neither by the growth on In$_x$Ga$_{1-x}$As (for $x \leqslant 0.31$), nor by the overgrowth of In$_x$Ga$_{1-x}$As upper confining layers (UCLs), if a low growth temperature is used [29,30]. This allows the exclusion of increased QD sizes, which can also result in a redshift of the emission, but may be deleterious as defects can emerge due to QD ripening [31].

In strain-engineered metamorphic QD systems the QD strain is tuned by controlling the QD-CL mismatch,

$$f = \frac{a_{\text{InAs}} - a_{\text{LCL}}}{a_{\text{LCL}}}. \tag{1}$$

a_{LCL} is the lattice parameter of partially relaxed In$_x$Ga$_{1-x}$As lower confining layer (LCL), and a_{InAs} is the lattice parameter of freestanding InAs. Note that a_{LCL} is a function of CL composition, but that it also depends on the LCL thickness. In the pseudomorphic growth regime a_{LCL} is equal to a_{GaAs}, the GaAs lattice parameter, but after a critical thickness for strain relaxation, d_c, is reached, it increases towards the freestanding value for In$_x$Ga$_{1-x}$As (metamorphic growth; see Fig. 1 of Ref. [17]). Hence, indium composition changes band discontinuities and QD-CL mismatch, while LCL thickness only directly affects the mismatch [32]. CL indium composition x and LCL thickness d can thus be used as two independent parameters to tune the emission energy [17].

It is clear that getting to 1.5 μm, or longer, by increasing the In composition in the CLs, and hence reducing band offset, reduces the confinement. Therefore, it is important to investigate exciton confinement in structures which emit at 1.5–1.6 μm. In particular, as the energy of the confined (electron) state approaches the (conduction) band offset; i.e., the localization energy approaches zero, the exciton wave function will spill over from the QD into the surrounding barrier material. Such spillover was already demonstrated, both theoretically and experimentally, in very flat InAs quantum wires in InP [33]. More recently, In-rich agglomerations in In$_x$Ga$_{1-x}$As were

found to be too small to confine electron states, even though zero-dimensional hole states were observed up to 400 K [34].

In this work we present low-temperature (2 K) magnetophotoluminescence (magneto-PL) studies of a series of samples with InAs QDs in metamorphic $In_xGa_{1-x}As$ confining layers. We use magneto-PL to extract information about the effect of changing CL composition x and LCL thickness d on exciton diamagnetic shift coefficient Γ, reduced mass μ, and Bohr radius a_B. We find that the reduced mass of the exciton initially increases with increasing QD-CL mismatch, but then saturates. The combined effects of decreasing localization energy (due to increasing x) and decreasing effective mass (due to decreasing mismatch), result in spillover of the exciton wave function. However, at the highest x of 0.35, an anomalous decrease in a_B is observed, which is attributed to a tendency for the experiment to measure smaller dots when the localization energy is very small.

II. EXPERIMENTAL DETAILS AND ANALYSIS METHOD

The $InAs/In_xGa_{1-x}As/GaAs$ samples studied in this work were grown by molecular beam epitaxy (MBE) on semi-insulating (100) GaAs substrates [17]. Growth started with a 100-nm-thick GaAs buffer layer deposited at 600 °C, followed by an $In_xGa_{1-x}As$ metamorphic LCL with fractional indium content x and thickness d, deposited at 490 °C by conventional MBE. After a growth interruption of 210 s, to lower the substrate temperature, InAs QDs with a nominal 3.0 ML coverage were grown by ALMBE at 460 °C. These were capped with a 20-nm-thick $In_xGa_{1-x}As$ upper confining layer (UCL) with the same composition as the LCL using ALMBE at 360 °C. Uncapped structures were grown under the same conditions for atomic force microscopy (AFM) characterization. This showed that the dot heights and diameters are 4.5 ± 1 nm and 22 ± 4 nm, respectively, and are independent of d and x for $x < 0.35$ (within the indicated range of confidence of AFM measurements), while their diameters increase to 31 ± 4 nm with heights unchanged for $x = 0.35$ (for the dominant size distribution) [29]. For our samples, transmission electron microscope measurements of capped QDs are very similar to AFM measurements of uncapped dots, in diameter and height [35]. In total, results from 29 samples are reported here (Table I), and in all but two cases ($x = 0.15$ with $d = 20$ nm, and $x = 0.24$ with $d = 10$ nm) d was thick enough for the LCL to reach the metamorphic growth regime.

Magnetophotoluminescence experiments were conducted using 40 mW (or, in cases where the PL intensity was low, 400 mW) of 532-nm light from a frequency-doubled neodymium-doped yttrium aluminum garnet (Nd:YAG) laser, transmitted via a 200-μm-core optical fiber. The laser spot on the sample surface was ~2 mm in diameter, resulting in laser power density that ranged from ~1 to ~10 W cm^{-2}. The sample was placed in the center of a solenoid magnet so that the magnetic field B was parallel to the growth direction z ($B//z$). When the magnetic field is applied, excitons are affected mainly through a compression of the wave function in the plane perpendicular to the applied field. Therefore, when examining the shift of the PL energy with $B//z$, the exciton radius in the plane of the sample can be determined. Two magnet systems were used. All samples were initially

measured in a dc superconducting magnet with a maximum field of 15 T. For about half of the samples in Table I this was sufficient to reach the high-field limit. For others a 50-T pulsed magnet was also available, but this was only suitable for samples with high PL intensity due to the short duration of the field pulse. In this comprehensive study, with a very large number of samples, there was no systematic difference in results obtained in the two magnet systems, other than the maximum field. The PL (Fig. 1) was collected via a 500-μm-core optical fiber and analyzed by a spectrometer of 30-cm focal length combined with an InGaAs diode array, sensitive between 900 and 1600 nm.

The so-called excitonic model [36] was used to determine the exciton properties: diamagnetic shift coefficient Γ, Bohr radius a_B, and reduced mass μ. The model categorizes the magnetic field dependence of the PL into two regimes: low and high field. The field regime depends upon the size of magnetic length, $l_B = \sqrt{\hbar/eB}$ (where $\hbar$, e, and B are the reduced Planck constant, electron charge, and magnetic field, respectively), relative to the Bohr radius of confined carriers in the plane perpendicular to the applied field. In the low-field regime, where the magnetic length is large compared with the exciton wave function, it causes only a small perturbation to orbital motion of the confined carriers; thus the spatial confinement dominates over the magnetic confinement. In this regime, the shift of PL energy, ΔE, is diamagnetic:

$$\Delta E = \Gamma B^2 = (e^2 a_B^2 / 8\mu) B^2. \tag{2}$$

In the high-field regime, where the magnetic length is smaller than the Bohr radius in the plane perpendicular to the applied magnetic field, magnetic confinement of carriers dominates, and the PL energy shifts linearly with field, following the lowest Landau level; i.e.,

$$\Delta E = (\hbar e / 2\mu) B. \tag{3}$$

The excitonic model assumes an instantaneous but smooth transition between the two regimes, such that equivalent expressions can be used to fit an entire set of PL energies E as a function of magnetic field in a single self-consistent process:

$$E = a_1 + a_2 B^2 \quad \text{for } B \leqslant B_c, \tag{4a}$$

and

$$E = a_1 - a_2 B_c^2 + 2a_2 B_c B \quad \text{for } B \geqslant B_c, \tag{4b}$$

where $a_1 = E_0$ (zero-field energy), $a_2 = (e^2 a_B^2)/8\mu$ (diamagnetic shift coefficient Γ) and B_c, which is the critical magnetic field at which the transition from the low-field to the high-field regime occurs, are fitting parameters. A detailed discussion of magneto-PL and the excitonic model can be found in the work of Hayne and Bansal [36].

In our work, there are two input experimental parameters: indium composition x and LCL thickness d, either or both of which are varied across the samples. The parameters which directly determine confinement properties are the band offset between QDs and CLs and the QD-CL mismatch, although, as mentioned above, there is not a one-to-one correspondence between them. We have analyzed our data by using the center

TABLE I. Sample design parameters, indium content x, and LCL thickness d, and the corresponding experimentally determined values of PL peak wavelength (10 K), diamagnetic shift coefficient Γ, reduced mass μ, and Bohr radius a_B (m_0 is the free electron mass). The final column records the type of setup used to acquire the respective data.

x	d (nm)	PL peak (nm)	$\Gamma(\mu\text{eV T}^{-2})$	$\mu(10^{-3}\,m_0)$	a_B(nm)	Field type
0.09	1000	1196	12.0 ± 0.5	77 ± 1	6.5 ± 0.2	Pulsed
0.12	165	1217	12.0 ± 0.2	86 ± 1	6.89 ± 0.02	Pulsed
0.15	20	1200	9.7 ± 0.3			dc
0.15	60	1232	12.3 ± 0.3			dc
0.15	60	1216	11.2 ± 0.5	79 ± 1	6.4 ± 0.2	Pulsed
0.15	60	1206	10.1 ± 0.4			dc
0.15	120	1237	10.2 ± 0.4	105 ± 3	6.97 ± 0.02	Pulsed
0.15	220	1254	17.8 ± 0.7	87 ± 1	8.4 ± 0.2	Pulsed
0.15	360	1268	17.2 ± 0.9	98.3 ± 8	8.8 ± 0.2	Pulsed
0.18	31	1216	14.04 ± 0.03			dc
0.2	547	1264	34.6 ± 0.5			dc
0.24	10	1222	17.8 ± 0.4			dc
0.24	70	1261	18 ± 1	67.8 ± 6	7.7 ± 0.2	Pulsed
0.24	145	1325	38 ± 2	135 ± 2	15.3 ± 0.3	dc
0.28	28	1273	11.5 ± 0.9			dc
0.28	37	1302	19.3 ± 0.9	68.1 ± 0.7	7.7 ± 0.2	Pulsed
0.28	60	1312	14.7 ± 0.9			dc
0.28	220	1337	70 ± 5	88 ± 2	16.9 ± 0.4	dc
0.28	220	1354	57 ± 4	89 ± 3	15.2 ± 0.6	dc
0.28	500	1343	72 ± 4	103.4 ± 0.9	18.4 ± 0.4	dc
0.31	60	1352	29.2 ± 0.4	95 ± 1	11.25 ± 0.06	dc
0.31	220	1362	113 ± 5	78.4 ± 0.2	20.1 ± 0.4	dc
0.31	500	1393	159 ± 5	71 ± 1	22.7 ± 0.6	dc
0.31	1000	1393	113 ± 7	44.9 ± 0.5	15.2 ± 0.4	dc
0.35	50	1447	47 ± 2	61 ± 2	11.5 ± 0.3	dc
0.35	60	1443	44 ± 3	63 ± 1	11.3 ± 0.2	dc
0.35	80	1455	43 ± 1	65 ± 1	11.2 ± 0.2	dc
0.35	220	1454	105 ± 8	24 ± 6	11 ± 1	dc
0.35	500	1496	114 ± 2	22 ± 1	10.7 ± 0.4	dc

of mass of the PL peak and extracting three output parameters from the magneto-PL: diamagnetic shift coefficient Γ, exciton Bohr radius a_B, and reduced mass of the exciton μ.

III. RESULTS AND DISCUSSIONS

A. Reduced mass and Bohr radius versus mismatch

Figure 2(a) shows exciton reduced mass as a function of QD-CL mismatch for samples whose PL energy shift reaches the high-field regime. As mismatch increases from 4.8% to 5.7%, the exciton reduced mass increases from the bulk InAs value of $0.02\,m_0$, then saturates at approximately $0.09\,m_0$ at higher mismatches. An increase of effective mass with strain (mismatch) is consistent with the theory reported in the literature [37,38], although it has not been discussed in detail, and the behavior observed in Fig. 2(a) has not been reported before, either theoretically or experimentally. The value of the exciton reduced mass is a combination of electron and hole masses, but will be dominated by the much lighter electron mass, and the observed change at low mismatch is quite remarkable (increasing by a factor of 4–5), so we hope that this result will stimulate further theoretical investigation.

Except for $x = 0.35$ [red data points in Fig. 2(b)], which will be discussed in detail in Sec. III C, the exciton Bohr radius

decreases with increasing mismatch up to 6.1%, then saturates [Fig. 2(b)]. The decrease in the Bohr radius with increasing mismatch can be attributed to improving confinement: The increasing mismatch (decreasing x) increases the barrier and the localization energy, and hence reduces the Bohr radius. Although the measured Bohr radius does not reach the bulk InAs value of 35 nm, at low mismatch ($\sim$5%) we see that it is double that of the dot radius (for $x < 0.35$). As In composition in the CLs is reduced (barrier height increased) a_B drops, and then saturates at a value of 70% of the dot radius (mismatch 6.1%–6.9%). This is clearly a transition from spillover of the exciton wave function [33,34] at low localization energy (low x and low barrier height), to a situation where the localization energy is sufficiently large that the exciton is fully confined, with a constant Bohr radius that is 70% of the dot radius, irrespective of further increases in barrier height (localization energy). Increases in effective mass with increasing mismatch [Fig. 2(a)] will also contribute to reducing the Bohr radius. Figure 2(b) thus directly traces the evolution from weak confinement (wave-function spillover), due to low localization energy, to strong confinement with large localization energy. We will return to the measurement of the Bohr radius (as a function of x and d) in Sec. III C, but first we discuss Γ (as a function of x and d), introducing the "bubble plot" representation of our results.
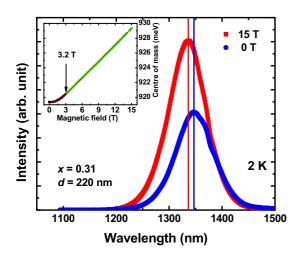
FIG. 1. Typical PL spectra, collected from a sample with $x = 0.31$ and $d = 220$ nm. The separation between vertical lines indicates the shift of the emission peak from 1347 nm at 0 T (blue), to 1336 nm at 15 T (red). The increase in PL intensity between 0 and 15 T results from field-induced compression of the exciton, increasing electron-hole wave-function overlap. The inset shows the dependence of the center of mass of the PL on magnetic field for the same sample. The arrow shows the crossover point, 3.2 T, from parabolic (black) to linear (green) behavior with magnetic field. The solid line (red) is the fit to the data according to Eq. (4).

B. Diamagnetic shift coefficient bubble plot

In our experiment there are two input parameters, x and d, and three output parameters, Γ, a_B, and μ, with Γ being a function of a_B and μ [Eq. (2)]. We have already presented a_B and μ as a function of lattice mismatch; however, mismatch is, itself, a function of the two input parameters x and d. It is therefore useful to see how the output parameters vary as a function of x and d, which can be conveniently done using a so-called bubble plot. We start by looking at the diamagnetic shift data, the results of which are summarized in Fig. 3, using this as an example to show the construction of the bubble plot. As discussed in Ref. [17], and confirmed experimentally in Ref. [30], when d exceeds the critical thickness for strain relaxation, d_c, the residual strain of the (partially) relaxed
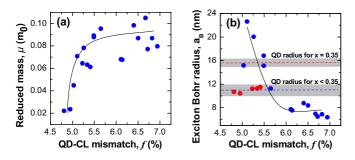

FIG. 2. (a) Reduced mass, μ, of the exciton increases with increasing QD-CL mismatch, then saturates. (b) Exciton Bohr radius decreases, except for $x = 0.35$ (red dots), with increasing mismatch and saturates at high mismatch. The dashed horizontal lines show the QD radii for $x = 0.35$ (red) and $x < 0.35$ (blue) [29]. The solid lines are a guide to the eye.
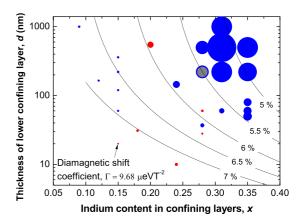

FIG. 3. Bubble plot showing relative values of diamagnetic shift coefficient Γ. The solid lines represent constant QD-CL mismatch f. For the two samples with the lowest LCL thickness, LCL growth was pseudomorphic, hence QD-CL mismatch is the maximum value of 7.16%. For the sample with $x = 0.15$ and $d = 20$ nm, $\Gamma = 9.68$ (μeV T^{-2}); the values for other samples are proportionally larger relative to the bubble diameter. Numerical values are listed in Table I. The blue/gray and red colors show the diamagnetic coefficient for samples reaching and not reaching the high-field regime, respectively.

In$_x$Ga$_{1-x}$As layers has a $d^{-1/2}$ dependence [39]. This allows a determination of the In$_x$Ga$_{1-x}$As in-plane lattice constant and, hence, the QD-CL mismatch f. It is instructive to plot lines of constant f in Fig. 3, calculated according to the model of Ref. [17]. Hence, by following these lines in Fig. 3 (and in Fig. 4), only the QD-CL band offset changes, while QD-CL mismatch remains constant.

Going horizontally from left to right along the graph (increasing indium content x, in CLs), both the band discontinuities between QDs and CLs, and lattice mismatch between QDs and CLs (thus strain), reduce. The mismatch also decreases while going up vertically (along increasing LCL
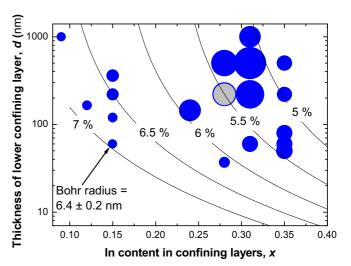

FIG. 4. Bubble plot showing the relative values of exciton Bohr radius as a function of indium content x in CLs, and of LCL thickness d for samples for which the high-field regime was reached. The arrow indicates the value of exciton Bohr radius for the sample with $x = 0.15$ and $d = 60$ nm. The lines show constant QD-CL mismatch f.

thickness), while band discontinuities are constant. We note that the strain does have an effect on the band discontinuities, but this is neglected.

The bubbles represent the relative values of diamagnetic shift coefficient by their diameters (diameter $\propto \Gamma$), which is a function of x and d. The samples are categorized into two groups, indicated by blue/gray and red bubbles, according to the behavior of PL energy shift in the magnetic field: the blue/gray colors represent the samples reaching the high-field regime (in either dc or pulsed magnet), i.e., where spatial confinement is dominated by magnetic confinement and ΔE becomes linear in high field. Likewise, samples not reaching the high-field regime are colored red.

For samples represented by blue/gray in Fig. 3, the magnetic field is sufficient to allow us to determine the exciton Bohr radius a_B, and reduced mass μ. The red bubbles represent the values of Γ for the samples where the exciton wave-function extent in the plane of the sample is smaller than the magnetic length at high field, and the energy shift remains parabolic. For these samples, we are unable to determine the exciton Bohr radius and reduced mass, but can still determine the diamagnetic coefficient Γ via Eq. (4a).

An immediately obvious and intriguing trend in Fig. 3 is the tenfold increase in the diamagnetic shift coefficient while going from $\sim 7\%$ to $\sim 5\%$ mismatch. This is the result of the combination of two effects. The first, discussed above with reference to Fig. 2(b), is the increasing spillover of the exciton wave function as we go from strong confinement of the excitons (large localization energy) at low x, to weak confinement (small localization energy) at high x. The second is the change in exciton mass: the low exciton mass at low QD-CL mismatch [Fig. 2(a)] will contribute to the wave-function spillover via an increase in the quantization energy, but it also has a direct effect on the diamagnetic shift [Eq. (2)].

C. Bohr radius bubble plot

Having introduced and explained the bubble plot, we can now discuss Bohr radius data in the same manner, which reveals some unexpected behavior. Figure 4 shows that a_B decreases with increasing barrier and mismatch, going horizontally from 0.31 to lower indium content for any particular LCL thickness. This is understandable, because increasing the barrier results in an increase of the localization energy which, in turn, improves confinement and hence reduces the Bohr radius, at least until the point where the Bohr radius is 70% of the dot size, as discussed earlier. Similarly, Fig. 2(a) shows that increasing mismatch tends to increase the exciton reduced mass, and since the exciton Bohr radius is inversely proportional to effective mass, this also tends to reduce the Bohr radius.

However, for $d > 100$ nm, going from $x = 0.35$ to $x = 0.31$, the opposite behavior is observed; i.e., at $x = 0.35$ a_B is apparently smaller than at $x = 0.31$ [see also Fig. 2(b)]. Furthermore, AFM measurements show that at $x = 0.35$, the QD diameter is actually bigger (31.3 ± 0.7 nm) than at $x = 0.31$ (22 ± 1 nm). Therefore, from the general trend in Fig. 4, wave-function spillover, and the decrease in the dot diameter, going from $x = 0.35$ to $x = 0.31$, we should certainly expect the Bohr radius at $x = 0.35$ to be larger than for lower x.

This can be explained with reference to the work of Nuytten *et al.* [40] An ensemble of self-assembled quantum dots always has a range of sizes. Warming the sample sufficiently causes a thermal redistribution of carriers from higher-energy (smaller) dots to lower-energy (bigger) dots via the wetting layer. This is manifested by the PL energy decreasing faster with increasing temperature than is expected from the change in the band gap [41–43]. Nuytten and co-workers studied the temperature dependence of the PL energy in magnetic field under such conditions [40], and concluded that for dots where such a redistribution of carriers occurs, in the presence of magnetic field, the contribution of the smaller dots (high-energy dots) to the PL energy becomes greater relative to the bigger dots (low-energy dots) as the field increases. Application of a magnetic field increases the energy gap between the states in QDs and the states of surrounding bulk material. This increase originates from the fact that the magnetic field raises the energy levels of the surrounding materials substantially, and the energy levels of the QDs moderately: The energy levels in the dots feel the confining effect of the field less due to the preexisting spatial confinement.

Furthermore, the effect of magnetic field on the energy levels depends upon the strength of exciton confinement in the dots. The field has a greater effect on the energy levels of dots with smaller confinement energy, i.e., bigger dots, than it does on dots with large confinement energy, i.e., smaller dots. Hence, for a given magnetic field, the energy levels in smaller dots are lifted much less than in bigger ones. Since the band offset (bulk/barrier level) is enhanced equally in both types of dots, by the application of a magnetic field, the localization energy for smaller dots is enhanced more than for bigger dots. Provided that carriers are able to thermally redistribute from larger dots (with relatively weakly field-enhanced localization energy) to smaller dots (with larger localization energy in the presence of magnetic field), the net result is that we tend to probe smaller dots in a magnetic field. This effect strengthens as temperature increases.

To investigate this further, we studied the temperature dependence of the PL energies for samples with $x = 0.35$ and $d > 100$ nm, and compared them with a sample at the opposite extreme, i.e., with $x = 0.15$ and $d = 20$ nm. The behavior of the zero-field PL energies with increasing temperature for both types of sample is shown in Fig. 5. The black and gray dashed lines show the Varshni dependences for InAs and GaAs, respectively [44]. For the $x = 0.15$ sample (green data in Fig. 5) the decrease in PL energy has the characteristic parabolic, then linear, Varshni form, although at high temperatures the change in energy is faster than would be expected for bulk InAs. In contrast, the two $x = 0.35$ samples (red and blue data in Fig. 5) show clearly anomalous behavior, with a very rapid decrease in PL energy that even exceeds expectations for bulk GaAs. Furthermore, the PL intensity quenches by 150 K. PL energy from self-assembled dots that decreases with increasing temperature faster than expected has been widely observed in the literature [40] and is interpreted as thermal redistribution of carriers from small dots to large dots (with lower PL energies) with increasing temperature (thermalization). Such a mechanism requires relatively weak confinement (low localization energy) to be observed at low temperatures. Hence this behavior is observed at $x = 0.35$,
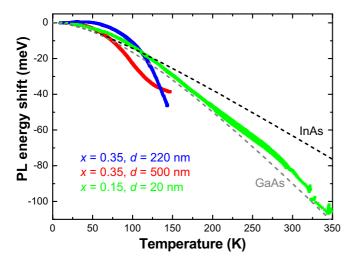
FIG. 5. PL energy shift versus temperature in zero field for samples with $x = 0.35$ and $d = 220$ nm (blue), $x = 0.35$ and $d = 500$ nm (red), and $x = 0.15$ and $d = 20$ nm (green). The PL energy for samples with $x = 0.35$ samples decreases rapidly with temperature, before being quenched above ~145 K. Black and gray dashed lines show the Varshni dependence for bulk InAs and GaAs, respectively [44].

and not at $x = 0.15$. It should also be noted that AFM characterization of metamorphic QDs highlighted an increase in the distribution of sizes (bimodal distribution) for QDs grown on $In_{0.35}Ga_{0.65}As$ (see Fig. 2 of Ref. [29]).

This explanation is reinforced by Fig. 6 which shows the shift of the PL energy between 0 and 15 T for the sample
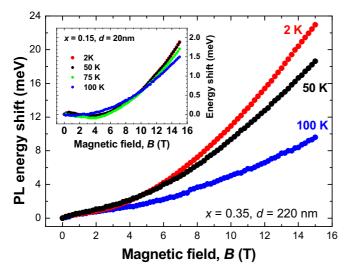

FIG. 6. PL energy shift versus magnetic field, B, at various temperatures: 2 K (red), 50 K (black), and 100 K (blue) for the sample with $x = 0.35$ and $d = 220$ nm. The figure shows that the energy shift decreases by a factor of ~2 with increasing temperature, from 2 to 100 K. Remarkably similar behavior was observed by Nuytten *et al.* [40]. The inset shows the behavior of PL energy at various temperatures in the presence of magnetic field for the sample with $x = 0.15$ and $d = 20$ nm. In this case there is no significant change in the magneto-PL as a function of temperature; indeed the 2 K data are almost totally obscured by the 50 K data.

with $x = 0.35$ and $d = 220$ nm at different temperatures. The size of the field-induced shift decreases by a factor of ~2 with increasing temperature from 2 to 100 K, and is remarkably similar to the behavior observed in Fig. 1 of Nuytten *et al.* [40]. In contrast, for the $x = 0.15$ sample, the data are essentially temperature independent up to 100 K.

Additional support for the existence of this mechanism is provided by estimating the relative changes of the various energy levels in a magnetic field. An estimate of the shift of the bulk levels in the barrier is found by using $\hbar E = \hbar \omega_c / 2$, where $\hbar \omega_c = eB/m^*$ and m^* is the electron effective mass in $In_{0.35}Ga_{0.65}As$, which is given by [44]

$$m_e = 0.023 + 0.037(1 - x) + 0.003(1 - x)^2 m_0. \quad (5)$$

Doing so, we find that the field enhancement of the bulk levels at 15 T is 18 meV. If we now equate the 2-K PL shift in magnetic field to that of bigger dots (actually it should be average), then the QD level shifts by 23 meV at 15 T (reading off from Fig. 6). This is similar to, indeed larger than, the shift of the bulk states; i.e., there can be little or no field-enhanced confinement effect. The shift at 100 K is attributed to much smaller dots, and is only 10 meV (Fig. 6). This is about half of the shift of the bulk states, adding 8 meV to the localization energy at 15 T.

Hence, for smaller dots the field increases the localization energy by at least 40% at 15 T, and has no, or a negligible, effect on large dots. At higher temperature, the contribution of the smaller dots to the PL becomes more prominent. In contrast, it is clear from the inset of Fig. 6 that the energy shift for the sample with $x = 0.15$ and $d = 20$ nm does not decrease significantly as temperature increases from 2 to 100 K. In such samples, all dots contribute to PL energy, even at 100 K. Thus, the reason for the radii being smaller at $x = 0.35$ than at $x = 0.31(d > 100$ nm) in Fig. 4 is the greater contribution of the smaller dots to the PL energy in a magnetic field, which results in smaller measured radii. It is also noticeable in Figs. 3 and 4 that the Bohr radius and diamagnetic shift for $x = 0.31$ and $d = 60$ nm are significantly smaller than for $x = 0.31$ and $d > 100$ nm, indicating that there is little or no wave-function spillover at $x = 0.31$ and $d = 60$ nm. Since the band offset is the same (same x) this can be attributed to a difference in mismatch affecting the effective mass.

IV. CONCLUSIONS

In this work we used magneto-PL to probe the exciton confinement in series of strain-engineered metamorphic $InAs/In_xGa_{1-x}As/GaAs$ QD samples for which the indium content in the confining layers (CLs) and the thickness of the lower confining layer were varied. We observed an increase of the exciton reduced mass with increasing strain (QD-CL mismatch) for mismatches in the 4.8%–5.7% range. At low QD-CL mismatch (large CL In content, low barrier height, low localization energy), we see clear spillover of the exciton wave function. This is suppressed at higher mismatches, as the In content in the CL decreases, and the barrier height and localization energy increase. The changes in effective mass and exciton Bohr radius together generate an order of magnitude

difference in the diamagnetic shift between samples with large and small mismatch. For samples with the largest CL In content (smallest barrier and localization energy) and smallest mismatch the magneto-PL appears to show an anomalous decrease in the Bohr radius. This is attributed to the combined effects of thermalization and field-enhanced confinement, the latter of which is stronger for smaller dots in the ensemble.

[1] D. Bimberg, M. Grundmann, and N. N. Ledentsov, *Quantum Dot Heterostructures* (Wiley, New York, 1999).

[2] N. N. Ledentsov *et al.*, J. Cryst. Growth **301–302**, 914 (2007).

[3] D. J. Mowbray and M. S. Skolnick, J. Phys. D: Appl. Phys. **38**, 2059 (2005).

[4] H. Naoto, F. Toshiro, N. Yoshiaki, Y. Naoki, M. Tanaya, and M. P. Pierre, Jpn. J. Appl. Phys. **38**, 2559 (1999).

[5] J. Tatebayashi, N. Hatori, H. Kakuma, H. Ebe, H. Sudo, A. Kuramata, Y. Nakata, M. Sugawara, and Y. Arakawa, Electron. Lett. **39**, 1130 (2003).

[6] T. Akiyama, H. Kuwatsuka, T. Simoyama, Y. Nakata, K. Mukai, M. Sugawara, O. Wada, and H. Ishikawa, IEEE J. Quantum Electron. **37**, 1059 (2001).

[7] M. Hayne, R. J. Young, E. P. Smakman, T. Nowozin, P. Hodgson, J. K. Garleff, P. Rambabu, P. M. Koenraad, A. Marent, L. Bonato, A. Schliwa, and D Bimberg, J. Phys. D: Appl. Phys. **46**, 264001 (2013).

[8] Z. Yuan, B. Kardynal, R. M. Stevenson, A. J. Shields, C. Lobo, K. Cooper, N. Beattie, D. A. Ritchie, and M. Pepper, Science **295**, 102 (2002).

[9] S. A. Chambers, Surf. Sci. Rep. **39**, 105 (2000).

[10] M. S. Skolnick and D. J. Mowbray, Annu. Rev. Mater. Res. **34**, 181 (2004).

[11] S. Fafard, K. Hinzer, S. Raymond, M. Dion, J. McCaffrey, Y. Feng, and S. Charbonneau, Science **274**, 1350 (1996).

[12] H.-Y. Liu, B. Xu, Y.-Q. Wei, D. Ding, J.-J. Qian, Q. Han, J.-B. Liang, and Z.-G. Wang, Appl. Phys. Lett. **79**, 2868 (2001).

[13] H. Y. Liu, D. T. Childs, T. J. Badcock, K. M. Groom, I. R. Sellers, M. Hopkinson, R. A. Hogg, D. J. Robbins, D. J. Mowbray, and M. S. Skolnick, IEEE Photon. Tech. Lett. **17**, 1139 (2005); C. Paranthoen, N. Bertru, B. Lambert, O. Dehaese, A. Le Corre, J. Even, S. Loualiche, F. Lissillour, G. Moreau, and J. C. Simon, Semicond. Sci Technol. **17**, L5 (2002).

[14] Z. Zhou, Y. Xu, R. Hao, B. Tang, Z. Ren, and Z. Niu, J. Appl. Phys. **103**, 094315 (2008).

[15] N. N. Ledentsov, Semicond. Sci. Technol. **26**, 014001 (2011).

[16] E. U. Rafailov, M. A. Cataluna, and W. Sibbett, Nat. Photon. **1**, 395 (2007).

[17] L. Seravalli, M. Minelli, P. Frigeri, S. Franchi, G. Guizzetti, M. Patrini, T. Ciabattoni, and M. Geddo, J. Appl. Phys. **101**, 024313 (2007).

[18] Y. Nakata, K. Mukai, M. Sugawara, K. Ohtsubo, H. Ishikawa, and N. Yokoyama, J. Cryst. Growth **208**, 93 (2000).

[19] M. J. da Silva, A. A. Quivy, S. Martini, T. E. Lamas, E. C. F. da Silva, and J. R. Leite, Appl. Phys. Lett. **82**, 2646 (2003).

[20] S. Franchi, G. Trevisi, L. Seravalli, and P. Frigeri, Prog. Cryst. Growth Charact. Mater. **47**, 166 (2003).

[21] E. C. Le Ru, A. J. Bennett, C. Roberts, and R. Murray, J. Appl. Phys. **91**, 1365 (2002).

[22] L. Bouzaiene, B. Ilahi, L. Sfaxi, F. Hassen, H. Maaref, O. Marty, and J. Dazord, Appl. Phys. A **79**, 587 (2004).

[23] L. Seravalli, M. Minelli, P. Frigeri, P. Allegri, V. Avanzini, and S. Franchi, Appl. Phys. Lett. **82**, 2341 (2003).

[24] Y.-C. Xin, L. G. Vaughn, L. R. Dawson, A. Stintz, Y. Lin, L. F. Lester, and D. L. Huffaker, J. Appl. Phys. **94**, 2133 (2003).

[25] L. Seravalli, P. Frigeri, M. Minelli, P. Allegri, V. Avanzini, and S. Franchi, Appl. Phys. Lett. **87**, 063101 (2005).

[26] Z. Mi and P. Bhattacharya, IEEE J. Sel. Top. Quantum Electron. **14**, 1171 (2008).

[27] L.Y. Karachinsky, T. Kettler, I. I. Novikov, Yu. M. Shernyakov, N. Yu. Gordeev, M. V. Maximov, N. V. Kryzhanovskaya, A. E. Zhuko, E. S. Semenova, A. P. Vasil'ev, V. M. Ustinov, G. Fiol, M. Kuntz, A. Lochmann, O. Schulz, L. Reissmann, K. Posilovic, A. R. Kovsh, S. S. Mikhrin, V. A. Shchukin *et al.*, Semicond. Sci. Technol. **21**, 691 (2006).

[28] G. Munoz-Matutano, D. Barrera, C. R. Fernandez-Pousa, R. Chulia-Jordan, L. Seravalli, G. Trevisi, P. Frigeri, S. Sales, and J. Martinez-Pastor, Sci. Rep. **6**, 27214 (2016).

[29] L. Seravalli, G. Trevisi, and P. Frigeri, CrystEngCommun **14**, 1155 (2012).

[30] V. Bellani, C. Bocchi, T. Ciabattoni, S. Franchi, P. Frigeri, P. Galinetto, M. Geddo, F. Germini, G. Guizzetti, L. Nasi, M. Patrini, L. Seravalli, and G. Trevisi, Eur. Phys. J. B **56**, 217 (2007).

[31] P. Frigeri, L. Nasi, M. Prezioso, L. Seravalli, G. Trevisi, E. Gombia, R. Mosca, F. Germini, C. Bocchi, and S. Franchi, J. Appl. Phys. **102**, 083506 (2007).

[32] Strain also indirectly affects the band discontinuities via its effect on the band structure, but this is a secondary effect.

[33] J. Maes, M. Hayne, Y. Sidor, B. Partoens, F. M. Peeters, Y. González, L. González, D. Fuster, J. M. Garcia, and V. V. Moshchalkov, Phys. Rev. B **70**, 155311 (2004); **76**, 199902(E) (2007).

[34] S. Harrison, M. P. Young, P. D. Hodgson, R. J. Young, M. Hayne, L. Danos, A. Schliwa, A. Strittmatter, A. Lenz, H. Eisele, U. W. Pohl, and D. Bimberg, Phys. Rev. B **93**, 085302 (2016).

[35] L. Seravalli, P. Frigeri, L. Nasi, G. Trevisi, and C. Bocchi, J. Appl. Phys. **108**, 064324 (2010).

[36] M. Hayne and B. Bansal, Luminescence **27**, 179 (2012).

[37] C. Pryor, Phys. Rev. B **57**, 7190 (1998).

[38] M. Yahyaoui, K. Sellami, S. B. Radhia, K. Boujdaria, M. Chamarro, B. Eble, C. Testelin, and A. Lemaître, Semicond. Sci. Technol. **29**, 075013 (2014).

[39] P. M. J. Marée, J. C. Barbour, J. F. van der Veen, K. L. Kavanagh, C. W. T. Bulle-Lieuwma, and M. P. A. Viegers, J. Appl. Phys. **62**, 4413 (1987).

[40] T. Nuytten, M. Hayne, M. Henini, and V. V. Moshchalkov, Phys. Rev. B **77**, 115348 (2008).

[41] P. Dawson, E. O. Göbel, K. Pierz, O. Rubel, S. D. Baranovskii, and P. Thomas, Phys. Status Solidi B **244**, 2803 (2007).

[42] L. Brusaferri, S. Sanguinetti, E. Grilli, M. Guzzi, A. Bignazzi, F. Bogani, L. Carraresi, M. Colocci, and A. Bosacchi, Appl. Phys. Lett. **69**, 3354 (1996).

[43] A. Polimeni, A. Patanè, M. Henini, L. Eaves, and P. C. Main, Phys. Rev. B **59**, 5064 (1999).

[44] I. Vurgaftman, J. R. Meyer, and L. R. Ram-Mohan, J. Appl. Phys. **89**, 5815 (2001).

[45] http://dx.doi.org/10.17635/lancaster/researchdata/183.